Semester Thesis

Computing electroweak quantum corrections using Local Unitarity

Maximilian Hofer, ETH Zürich
hoferma@student.ethz.ch

July 21, 2022

Abstract

In this semester thesis we compute the differential cross-section and forward-backward asymmetry of the process $e^+e^- \to \gamma/Z \to t\bar{t}(g)$ up to next-to-leading order using Local Unitarity (LU). The numerical results are consistent with those produced using MadGraph5_aMC@NLO and therefore constitute the first successful application of LU to the electroweak sector. Apart from presenting the results we also provide a very basic introduction to LU and to the difficulties regarding the treatment of the fifth gamma matrix in dimensional regularization.

1 Introduction

The forward-backward asymmetry (AFB) has always been an important observable in the investigation of weak neutral currents as it is sensitive to terms that are odd in $\cos\theta$ which drop out in the integrated cross-section. Because such terms can only occur in chiral theories, the AFB allows measuring effects of weak interactions already at energies way below the Z mass and already at leading order (LO). Indeed, even before the discovery of the Z boson in 1983 a non-zero AFB could be measured at an energy of $\sqrt{s} = 34.5\,\text{GeV}$ at PETRA to give early evidence for the electroweak structure. A more recent example explaining the interest in this physical quantity comes from measurements of the bottom quark in which the AFB showed a discrepancy of 2.8 standard deviations from the Standard Model predictions. Although this result was published in 2005 (and apart from a reduction to $2.4\,\sigma$), it is still not understood where the origin of this discrepancy is to be found (see [1] and

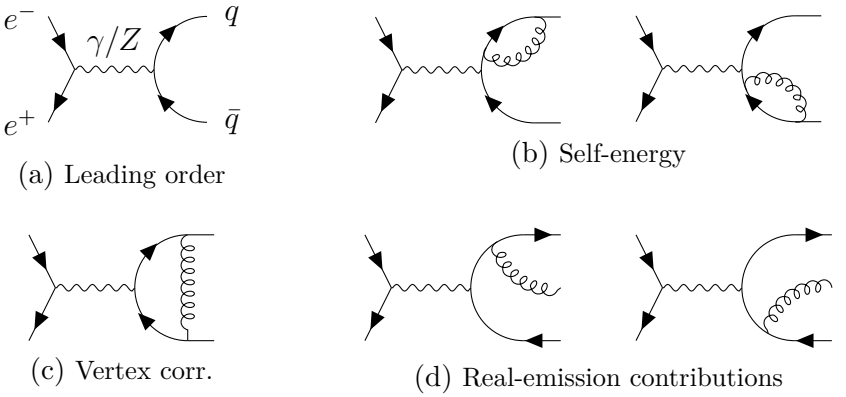

(a) Leading order

(b) Self-energy

(c) Vertex corr.

(d) Real-emission contributions

Figure 1: Amplitude diagrams for the process $e^+e^- \to q\bar{q}$ up to NLO. Notice that there are in total 12 diagrams because each one comes once with the photon and once with the Z boson as exchange particle.

references therein). While future e^+e^- colliders will hopefully increase the experimental precision, it is also necessary to push the theoretical predictions beyond the current state of the art to the three-loop level.

A promising route to achieve this goal is given by Local Unitarity [2], a relatively new approach to perturbative quantum field theory (QFT) in which the differential cross-section is represented in a way such that the cancellation of infrared (IR) singularities takes place already at the local level. This permits a fully numerical treatment which is not only generalizable to arbitrary orders but also facilitates the handling of observables. This semester thesis makes a first modest step on the way to reaching the aforementioned goal in computing the forward-backward asymmetry of $e^+e^- \to \gamma/Z \to t\bar{t}(g)$ at next-to-leading order (NLO) using Local Unitarity.

In the following section we will introduce Local Unitarity, give some technical details on the implementation of the fifth gamma matrix and define and discuss the AFB observable. The numerical results are presented in Section 3. Finally, a conclusion is drawn and some prospects for future work is given in Section 4.

2 Methods

2.1 Local Unitarity

In order to work with the process $e^+e^- \to \gamma/Z \to q\bar{q}(g)$, traditional approaches to perturbative QFT would require us to first draw the diagrams for the amplitudes up to NLO as in Figure 1. The diagrams in the second row are

all IR divergent but when combined they result in a finite quantity. On the integrated level this circumstance is known as the Kinoshita-Lee-Nauenberg (KLN) theorem [3, 4]. This fact is highly non-trivial as the diagrams 1c and 1d have a very different structure: The former encodes a loop integral over four-dimensional Minkowski space while the latter is a phase space integral over three-dimensional Euclidean space. In practice this means that one first has to temporarily regulate the IR divergences so that both integrals can be evaluated separately with different techniques appropriate to the different types. Only in the very end they are combined such that the cancellation of singularities can finally take place and the regulator can be removed.

Arguably this procedure is fairly unnatural as it ignores the intimate connection between virtual degrees of freedom and real-emission contributions. As it turns out, this relation goes even deeper than the KLN theorem suggests because the IR cancellations actually happen already on the differential level. This observation is the idea behind Local Unitarity (LU). More precisely, LU describes a representation of differential cross-sections that makes these local cancellations apparent. This allows a unified treatment of all IR divergences, thereby avoiding most of the difficulties that commonly arise in the traditional paradigm that was sketched in the previous paragraph.

A first step towards LU is to part with amplitudes and instead look at the interference terms in the absolute square of the amplitude. Diagrammatically, this means to glue amplitude diagrams together. For instance, a particular interference term of the process at hand would be

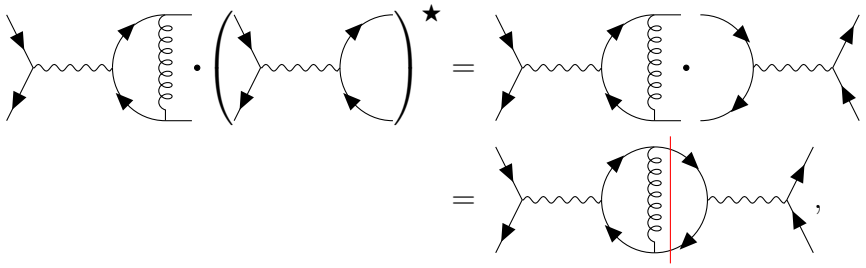

where in the second line we have rewritten the interference term as a *Cutkosky cut* (red line) of the *supergraph* depicted in Figure 2b. A Cutkosky cut is basically defined through the above equation in that it cuts a supergraph into two distinct, connected amplitude diagrams and puts the propagators it traverses onto the mass-shell. As it turns out, all the interference terms that can be constructed from the amplitude diagrams in Figure 1 can be obtained by applying all possible Cutkosky cuts[1] to all the supergraphs in Figure 2.

[1]except for some that e.g. have no phase space support like the one cutting only a Z propagator in the above diagrams.

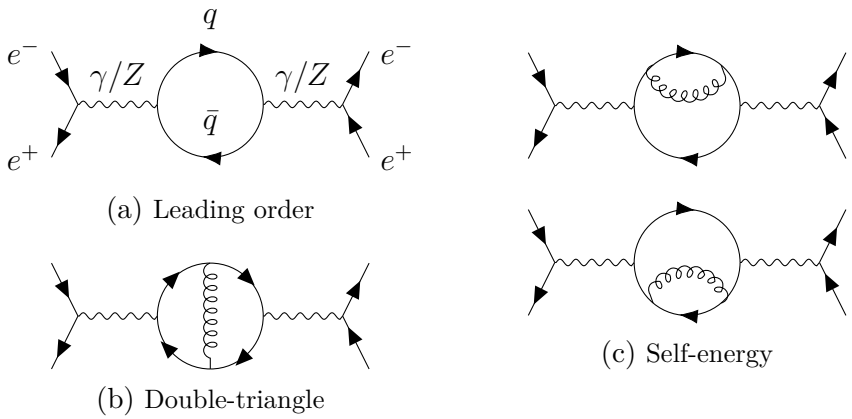

(a) Leading order

(b) Double-triangle

(c) Self-energy

Figure 2: Supergraphs of the process $e^+e^- \to q\bar{q}$ up to NLO. There are in total 16 graphs because each of the exchange bosons can be either a photon or a Z boson.

So what is gained by looking at supergraphs instead of amplitude diagrams? The point is that each supergraph − with that we now mean the sum over all its Cutkosky cuts − is locally IR finite. A proof of this fundamental statement under more general conditions (e.g. for arbitrary order and number of initial states) is provided in Section 3.2 of [2]. Essentially it is conducted by explicitly showing how one can align the integration measures between the different Cutkosky cuts and in particular between real and virtual contributions.

To resolve the aforementioned issue that these types don't even share the same dimensionality, a further ingredient called *Loop-Tree Duality* (LTD) comes into play (first proposed in [5], generalized to arbitrary orders and topologies in [6, 7]). As the name suggests, this identity allows to rewrite a loop integral as a sum over tree-like integrals. It does so by repeatedly applying the residue theorem to explicitly integrate out the energy components of the loop (four-)momenta. This leverages the fact that the pole structure is only determined by the denominators which are rather simple as they typically contain only factors of the form $q^2 - m^2 \pm i\delta$ (where q is the momentum of the propagator). The result is a sum of residues which are essentially obtained by removing a pole and evaluating the remaining function at this pole. Physically, this means that the particle corresponding to the propagator is put on-shell which as we have already seen can be visualized by a cut (in blue below) in the diagram. For instance (only applied to left subgraph):

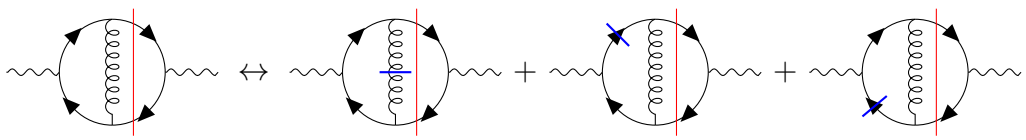

At higher order (e.g. when applied to the full double-triangle without the red Cutkosky cut), there is one cut for each independent loop momentum (see the next example). The independence means that if we were to remove the cut propagators we would not only be left with a tree, but a spanning tree of the (sub)graph to which LTD was applied.

The tree-like diagrams still become singular when propagators that are not cut go on-shell. This condition can be written in terms of the loop (three-)momenta and the incoming momentum by plugging

$$E_i(\vec{q}) := \sqrt{||\vec{q}||^2 + m_i}$$

into the relevant energy conservation relation. To make this concrete, consider the following contribution to the LTD representation of the double-triangle supergraph:

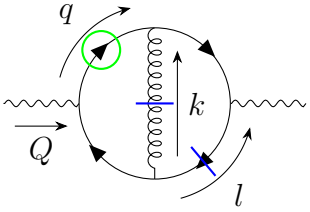

For the encircled propagator to go on-shell we need $q^0 = E_q(\vec{q})$, where we reused the momentum label as an index for the propagator. Energy conservation for the propagators of interest gives $Q^0 = q^0 + l^0 + k^0$ and by taking into account that Q, k and l are on-shell, we can write the condition as

$$\eta(\vec{k}, \vec{l}) := E_q\left(\vec{q}(\vec{k}, \vec{l})\right) + E_k(\vec{k}) + E_l(\vec{l}) - Q^0 = 0.$$

Because the signs in front of the E_i are all positive, this equation geometrically describes a convex and bounded surface in momentum space resembling an ellipsoid. It is therefore called an *E-surface*. The residue theorem also produces terms with singular surfaces for which the signs in the defining equation vary. These surfaces are of hyperboloidal shape and are thus denoted *H-surfaces*. It turns out that there are actually no H-surfaces in the dual integrand of LTD thanks to what is known as *dual cancellations* [8, 9]. On the other hand, E-surfaces are in general present in the LTD expression but cancel in the LU representation upon summation over the various Cutkosky cuts. The reason for this is the close relation between cuts and singularities, as both amount to putting a propagator on-shell. For example, the contributions

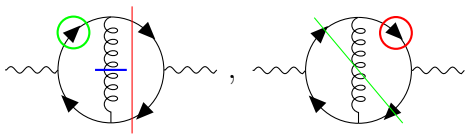

cancel when the encircled propagators become on-shell (which is reasonable because it means that the same propagators on the left are on-shell as on the right). A similar pairing exists for all the Cutkosky cuts and E-surfaces, so that all IR-singularities are removed, at least in the inclusive case. We will shortly discuss what has to be considered when observables like the forward-backward asymmetry come into play, but let us first return to the main objective of aligning the integration measure.

To this end, what remains to do is solving the delta functions coming from the on-shell conditions imposed by the Cutkosky cuts. Since the energy variables of the cut propagators are not all independent due to energy conservation, they cannot be solved directly. Instead, a mathematical trick called *the causal flow* is applied. The basic idea is to introduce a new variable t by inserting a 1 in the form of $1 = \int_{-\infty}^{\infty} \mathrm{d}t\, h(t)$ for some appropriately chosen function $h(t)$. A substitution of the integration variables $\vec{k}, \vec{l}, \dots$ using a specific mathematical flow $\phi^t : (\vec{k}, \vec{l}, \dots) \mapsto \phi(t, \vec{k}, \vec{l}, \dots)$ subsequently brings t into the arguments of the delta functions which permits solving them using the integration over t.

The result of the outlined procedure is a representation of the cross-section σ in the form

$$\sigma = \sum_{L=1}^{\infty} \alpha_s^L \int \mathrm{d}\Pi_L(x)\, f^{(L)}(x),$$

where at every order L there is only one overall integration measure $\mathrm{d}\Pi_L(x)$ over an integrand $f^{(L)}$ that is free of IR singularities. This not only allows a direct computation using Monte Carlo (MC) integration, but makes the extension to arbitrary (but IR-safe, see below) observables $\mathcal{O}(x)$ trivial by means of a simple replacement $f^{(L)} \to \mathcal{O} f^{(L)}$. This is not only straightforward but also convenient in terms of the implementation as it simply requires different weights in the MC integration. Thus, multiple observables can be evaluated at once for each sample point with almost no additional overhead.

However, the extension to observables also entails a problem, namely that they generally depend on the cut and thus spoil the cancellation of E-surfaces. In this case, the integration can still be performed by applying a contour deformation[2] $\vec{k} \to \vec{k} - i\vec{\kappa}$ which has to satisfy several properties described in [7] in order not to affect the result. For instance, on E-surfaces, the projection $\vec{\kappa} \cdot \vec{\nabla}\eta$ of $\vec{\kappa}$ onto the surface normal $\vec{\nabla}\eta$ must always have a positive sign (i.e. κ must point outwards of the surfaces, c.f. Figure 3) so that it does not interfere with the causal $\pm i\delta$ prescription. However, not every E-surface

[2] $\vec{k} \in \mathbb{R}^{3L}$ denotes now the direct sum of all L loop momenta.

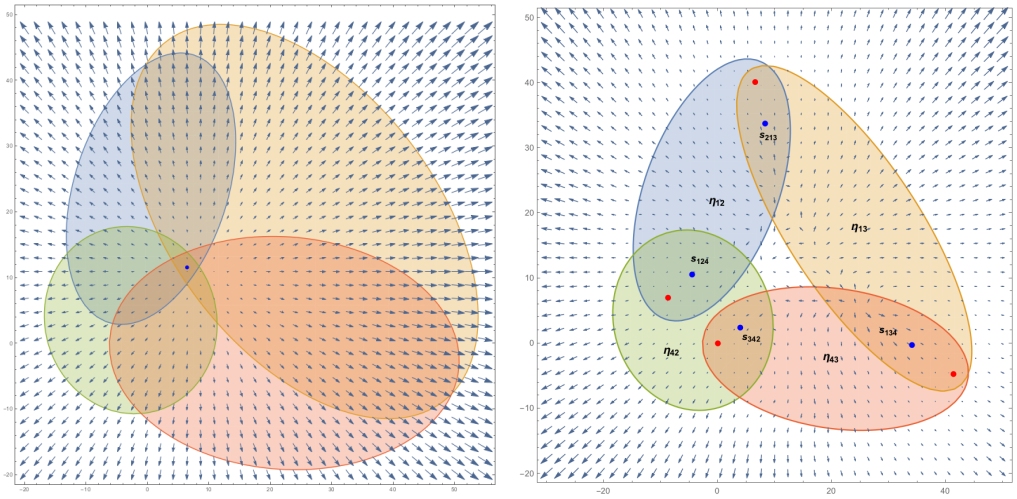

Figure 3: Visualization of the deformation field κ (diagrams from [7]). On the left, the interiors of the E-surfaces have one point in common, so the causal constraint can easily be satisfied by choosing $\vec{\kappa}$ to point radially outwards. On the right, a more complicated case is shown where a weighted combination of multiple radial fields with different sources is used. Details on how this is done are given in [7].

can be deformed around and in that case we speak of a *pinched* E-surface. For this reason, an observable can only be considered IR-safe if it does not prevent the cancellation of pinched E-surfaces. Conditions for which this holds true are discussed in [2, Section 3.2.5]. Finally, notice that for the cancellation of pinched E-surfaces it is also necessary that the deformation vanishes on these surfaces, and it must do so faster than the surface $\eta(\vec{k})$ itself. Otherwise, the cancellation between the non-deformed real-emission and the deformed virtual graphs cannot take place.

The preceding description of the intriguing ideas behind Local Unitarity was obviously sketchy and missing out on many other interesting aspects. For a more detailed yet still rather short introduction we recommend [10]. To study the theory in all its details and with full mathematical rigor we refer again to the main paper [2].

2.2 Implementation of fifth gamma matrix

The program outlined in the previous section is of course very extensive and transferring it into functioning code that is as generically applicable as the underlying method itself is a Herculean task that will take years to complete. While so far the current implementation of LU which is called

αLoop has mainly been applied to QCD and QED processes, the work carried out for this semester thesis took the first step towards the electroweak sector by adding the Z boson together with some functionality to handle the γ^5 matrix as well as the AFB observable. We will now give some details about the second aspect, intended as a summary of what has been done and what still needs to be done.

In four dimensional space-time, the fifth gamma matrix is typically defined as

$$\gamma^5 = i\gamma^0\gamma^1\gamma^2\gamma^3$$

or equivalently

$$\gamma^5 = \frac{i}{4!}\varepsilon_{\mu\nu\rho\sigma}\gamma^\mu\gamma^\nu\gamma^\rho\gamma^\sigma. \tag{1}$$

It has the following important properties:

$$\left(\gamma^5\right)^2 = 1, \qquad \{\gamma^5, \gamma^\mu\} = 0, \quad \mu = 0, 1, 2, 3 \tag{2}$$

The problem arises now in dimensional regularization[3] because it is not clear what the "correct" way to generalize either of the above definitions to $D = 4-2\epsilon$ dimensions is. In fact, since the Levi-Civita tensor is an inherently four-dimensional object, it turns out that there is no generalization that preserves all the properties we are used to at four dimensions. A straightforward try would be to just reuse the exact same form (1) and in particular to keep the summation of indices only over integer ones. By using $\{\gamma^\mu, \gamma^\nu\} = 2g^{\mu\nu}$ this would imply the typical $\{\gamma^\mu, \gamma^5\} = 0$ if $\mu \in \{0, 1, 2, 3\}$ but at the same time $[\gamma^\mu, \gamma^5] = 0$ for non-integer μ. This leads to a consistent scheme and was in fact already discussed in Section 6 of the original paper on dimensional regularization from 1972 by 't Hooft and Veltman [12]. There the authors provide an example showing that in diagrams exhibiting anomalies this definition of γ^5 can lead to a violation of the Ward identities. Another γ^5 scheme that does not have this caveat was proposed in 1991 by Körner, Kreimer and Schlicher (KKS) [13]. It is based on enforcing $\{\gamma^5, \gamma^\mu\} = 0$ for all (possibly non-integer) μ, which comes however at the price that the Dirac trace is no longer cyclic. All of these issues manifest themselves only really in graphs with anomalous behavior, so the implementation can only be completed upon careful study and testing of these cases.

For the process we are concerned with in this work most of these subtleties can be ignored and the scheme that is currently used was primarily chosen for its simple and flexible implementation. Given a "gamma string", by which

[3]Notice that even though LU does not need any regularization procedure for infrared singularities, dimensional regularization is still required for the renormalization of UV singularities. Details of how renormalization is handled within LU can be found in [11].

we mean a product of gamma matrices in index notation[4] like $\gamma^\mu_{ab}\gamma^5_{bc}\gamma^\nu_{cd}$, the algorithm works as follows:

- Apply $\{\gamma^5, \gamma^\mu\} = 0$ to repeatedly move γ^5 to the left, until any of the following applies or γ^5 is already at the very left.
  - If two γ^5 matrices are adjacent, apply $(\gamma^5)^2 = 1$ to remove them.
  - If there is a gamma string of the form $\gamma^{\mu_1}_{a_1a_2} \cdots \gamma^{\mu_n}_{a_na_1}$, solve this trace as usually when there is no γ^5 (in particular, set it to zero if n is odd).
  - If there is a gamma string of the form $\gamma^{\mu_1}_{a_1a_2} \cdots \gamma^{\mu_n}_{a_nb}\gamma^5_{ba_1}$, set it to zero if n is odd, otherwise substitute (1) and then solve the remaining trace as usually when there is no γ^5.
- Repeat the previous step until it has no effect anymore.

This scheme is more reminiscent of the second one (KKS) we mentioned before in that it makes use of anti-commutativity for γ^5. However, it still differs in that it eventually does perform the substitution (1) (while the other scheme uses additional trace rules for γ^5). Whether this could make a difference in some cases has yet to be investigated. We conclude this section with a remark on a potential source for error. Notice that $\gamma^{\mu_1}_{a_1a_2} \cdots \gamma^{\mu_n}_{a_nb}\gamma^5_{ba_1}$ is the same as $\gamma^5_{ba_1}\gamma^{\mu_1}_{a_1a_2} \cdots \gamma^{\mu_n}_{a_nb}$, so the placement of γ^5 in the trace is not fully defined by the algorithm. Since the cyclicity is no longer given in the KKS scheme, this could become an issue in some edge cases.

2.3 The forward-backward asymmetry

The forward-backward asymmetry A_{FB} is defined as

$$A_{\mathrm{FB}} = \frac{\sigma_F - \sigma_B}{\sigma_F + \sigma_B}, \tag{3}$$

where σ_F (σ_B) is the contribution to the total cross-section in "forward" ("backward") direction, or more precisely,

$$\sigma_F = \int_0^1 \mathrm{d}\cos\theta \, \frac{\mathrm{d}\sigma}{\mathrm{d}\cos\theta}, \quad \sigma_B = \int_{-1}^0 \mathrm{d}\cos\theta \, \frac{\mathrm{d}\sigma}{\mathrm{d}\cos\theta}.$$

Here, θ is the angle between the directions of flight of the initial state electron and the final state quark. Other choices for the reference axis like the

[4]The index notation is used because it allows working with commuting objects and also because it leads to an equal treatment of products and traces of gamma matrices.

thrust axis might be preferable when comparing with experiments but for our purposes the distinction is insignificant[5].

Now that the observable A_{FB} is defined, let us understand why it deviates from zero in the process $e^+e^- \to \gamma/Z \to q\bar{q}$ but not without the Z boson. The fundamental difference is that the QED vertex is invariant under a parity transformation while the electroweak Z-fermion-fermion vertex,

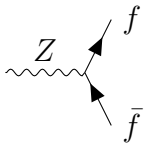

$$\propto c_V^f \gamma^\mu + c_A^f \gamma^5 \gamma^\mu,$$

mixes vector (γ^μ) and axial vector ($\gamma^\mu\gamma^5$) currents and therefore is not invariant. To see how this mixture affects the cross-section, consider again the leading order supergraph from Figure 2a:

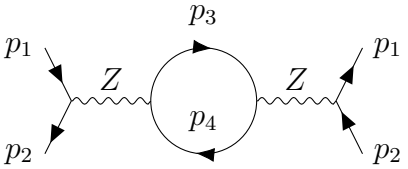

The momenta shall all be oriented such that they point from left to the right. The photon contribution can be neglected as it effectively just leads to a change in the constant c_V^f. Setting at first $m_e = m_q = 0$, we find in the Feynman gauge that the numerator is up to a constant factor equal to

$$\mathrm{tr}\left(\not{p}_1(c_V^e + c_A^e\gamma^5)\gamma^\mu \not{p}_2(c_V^e + c_A^e\gamma^5)\gamma^\nu\right) \mathrm{tr}\left(\not{p}_3(c_V^q + c_A^q\gamma^5)\gamma_\nu \not{p}_4(c_V^q + c_A^q\gamma^5)\gamma_\mu\right).$$

In order to solve this trace it is convenient to pair up the factors $(c_V^f + c_A^f\gamma^5)$ using $\{\gamma^\mu, \gamma^5\} = 0$. Although we wrote down the traces for the LO supergraph for concreteness, the same can be done for the other diagrams in Figure 2. The only difference lies in the number of times the anti-commutation relation has to be applied. Once the factors are paired up, they can be simplified using $(\gamma^5)^2 = 1$:

$$(c_V^f + c_A^f\gamma^5)(c_V^f \pm c_A^f\gamma^5) = (c_V^f)^2 + c_A^f c_V^f(1 \pm 1)\gamma^5 \pm (c_A^f)^2, \tag{4}$$

where the sign depends on whether there is an even (+) or odd (−) number of gamma matrices between the $(c_V^f + c_A^f\gamma^5)$ factors. There can only be a

[5]For example, in a comparison of these two choices for the b-quark in [1, Table 4], the difference at NLO was less than one per mill.

forward-backward asymmetry if γ^5 contributes to at least one of the traces (as otherwise it is effectively just QED with a different coupling constant), so we need that both c_A^f and c_V^f are non-zero and that the plus sign appears in at least one trace. In the leading order supergraph from above we see that the plus sign actually appears in both traces. In fact, this does not change at higher order as the addition of a QED-like vertex in the fermion loop comes with two gamma matrices (one from the vertex, one because the propagator gets split into two). The minus sign can occur in the massive case where there are additional terms obtained by replacing some momenta $\not{p}_i$ by a mass $m_{e/q}$.

Since we are only considering final state radiation, the electron trace remains the same at any order, so it is worth looking at the exact form of its trace (now with masses included):

$$\begin{aligned} T_e^{\mu\nu}(p_1,p_2) &:= \operatorname{tr}\left((\not{p}_1 + m_e)(c_V^e + c_A^e\gamma^5)\gamma^\mu(\not{p}_2 - m_e)(c_V^e + c_A^e\gamma^5)\gamma^\nu\right) \\ &= 4\left((c_V^e)^2 + (c_A^e)^2\right)(p_1^\mu p_2^\nu + p_1^\nu p_2^\mu - p_1\cdot p_2 g^{\mu\nu}) \\ &\quad + 4\left((c_A^e)^2 - (c_V^e)^2\right)m_e^2 g^{\mu\nu} + 8ic_V^e c_A^e \epsilon^{\alpha\beta\mu\nu} p_{1\alpha} p_{2\beta} \end{aligned}$$

Comparing the coefficients with (4) confirms that the only term coming from a trace containing γ^5 is the very last one. Of course this can also be seen from the Levi-Civita symbol. Notice how this term is antisymmetric in both (μ,ν) and (p_1,p_2), while all other terms are symmetric in both pairs. Since an exchange $p_1 \leftrightarrow p_2$ just amounts to $\cos\theta \to -\cos\theta$ (in the center-of-mass frame), this is indeed the term responsible for asymmetry. That μ and ν have the same (anti)symmetry structure as p_1 and p_2 is a consequence of the cyclicity of the trace and can be seen diagrammatically by relabeling p_1 and p_2 and attaching the boson lines at the opposite vertex, which leaves the diagram invariant.

At leading order, the quark loop has the same structure as the electron loop, so that the contraction of both traces is just $T_e^{\mu\nu}(p_1,p_2)T_{q,\nu\mu}(p_3.p_4)$. From the discussion above it follows that the terms (anti)symmetric in (p_1,p_2) can even be computed separately but just contracting the (anti)symmetric parts of the tensors (with respect to (μ,ν)). This also holds at higher order as it already follows from the properties of the electron trace. The forward-backward asymmetry at leading order can now be computed as

$$A_{FB}^{LO} = \frac{\left(\int_0^1 \mathrm{d}\cos\theta - \int_{-1}^0 \mathrm{d}\cos\theta\right) T_e^{\mu\nu}(p_1,p_2)T_{q,\nu\mu}(p_3.p_4)}{\int_{-1}^1 \mathrm{d}\cos\theta\, T_e^{\mu\nu}(p_1,p_2)T_{q,\nu\mu}(p_3.p_4)}.$$

For a comparison with the numerical results (see Figure 4) in the next section

we provide the result in the case $m_e = 0$:

$$A_{FB}^{LO}(s) = \frac{3c_V^e c_A^e c_V^q c_A^q \sqrt{s}\sqrt{s-4m_q^2}}{((c_A^e)^2 + (c_V^e)^2)\left[(c_A^q)^2(s-4m_q^2) + (c_V^q)^2(s+2m_q^2)\right]} \tag{5}$$

The values of the coefficients are $c_V^e = -\frac{1}{2} + 2\sin^2\theta_W$, $c_A^e = -\frac{1}{2}$, $c_V^t = \frac{1}{2} - \frac{4}{3}\sin^2\theta_W$, $c_A^t = \frac{1}{2}$ (taken from [14]). To take the photon contribution into account, one simply has to replace $c_V^f \to c_V^f + 2Q_f \cos\theta_W \sin\theta_W$ where $Q_e = -1$ and $Q_t = \frac{2}{3}$. Finally, notice that in the limit $m_q \to 0$ (or $s \gg m_q^2$) eq. (5) becomes independent of s:

$$\lim_{m_q \to 0} A_{FB}^{LO}(s) = \frac{3c_V^e c_A^e c_V^q c_A^q}{((c_A^e)^2 + (c_V^e)^2)((c_A^q)^2 + (c_V^q)^2)}$$

3 Numerical results

In the following section we present our results for the process $e^+e^- \to t\bar{t}(g)$ produced with the Local Unitarity implementation αLoop. In each case we use MadGraph5_aMC@NLO [15, 16] for comparison. The main result is the computation of the forward-backward asymmetries A_{FB} (as defined in (3)) at different center-of-mass energies $\sqrt{s}$. The numbers are given in Table 1 together with the total cross-sections. Graphical representations of these data are provided in Figures 4 and 7. A closer look at the angular dependence of the differential cross-section is given in Figures 5 and 6 for the cases $\sqrt{s} = 400\,\text{GeV}$ and $\sqrt{s} = 700\,\text{GeV}$ respectively. Notice that A_{FB}^{NLO} always denotes the forward-backward asymmetry when considering all LO **and** NLO diagrams combined while σ^{NLO} means the pure NLO contribution to the cross-section. In all cases the renormalization scale was set to the Z mass. The uncertainties were propagated using `python`'s `uncertainties` package [17]. The values of the relevant physical parameters that were used are given in Table 2.

$\sqrt{s}$ [GeV]	tool	A_{FB}^{LO}[%]	A_{FB}^{NLO}[%]	σ^{LO} [pb]	σ^{NLO} [pb]
360	αLoop	15.34	15.76	0.4347	0.3137
360	MG5	15.34(1)	15.77(1)	0.4347	0.3138
400	αLoop	28.23	29.11(1)	0.6231	0.1973(1)
400	MG5	28.23(1)	29.10(1)	0.6231(1)	0.1974
450	αLoop	36.44	37.46(1)	0.6116	0.1250(1)
450	MG5	36.46(1)	37.49(1)	0.6116	0.1251
500	αLoop	41.62	42.62	0.5486	0.08539(3)
500	MG5	41.61(1)	42.62(1)	0.5486	0.08537(2)
550	αLoop	45.21	46.10(2)	0.4809	0.06157(15)
550	MG5	45.20	46.12	0.4810	0.06143(1)
600	αLoop	47.84	48.63(2)	0.4198	0.04604(12)
600	MG5	47.86(2)	48.66(2)	0.4198(1)	0.04605(4)
650	αLoop	49.85	50.53(2)	0.3672	0.03570(9)
650	MG5	49.85(1)	50.53(1)	0.3672	0.03564(2)
700	αLoop	51.50(1)	52.04(2)	0.3226(1)	0.02827(3)
700	MG5	51.44(1)	51.98(1)	0.3227	0.02830(1)

Table 1: Forward-backward asymmetries and differential cross-sections of the process $e^+e^- \to \gamma/Z \to t\bar{t}(g)$ at leading (LO) and next-to-leading order (NLO). Missing uncertainties mean they were smaller than the error from rounding to four significant digits.

Parameter	Symbol	Value
Z mass	M_Z	91.188 GeV
Top mass	M_t	173 GeV
Higgs mass	M_H	125 GeV
Electron mass	m_e	0
QED coupling	$1/\alpha(\mu = M_Z)$	132.507
Strong coupling	$\alpha_s(\mu = M_Z)$	0.118
Fermi constant	G_F	$1.16639 \cdot 10^{-5}\,\text{GeV}^{-2}$

Table 2: Independent physical parameters that have been used. Other quantities like the Weinberg angle were derived from those.

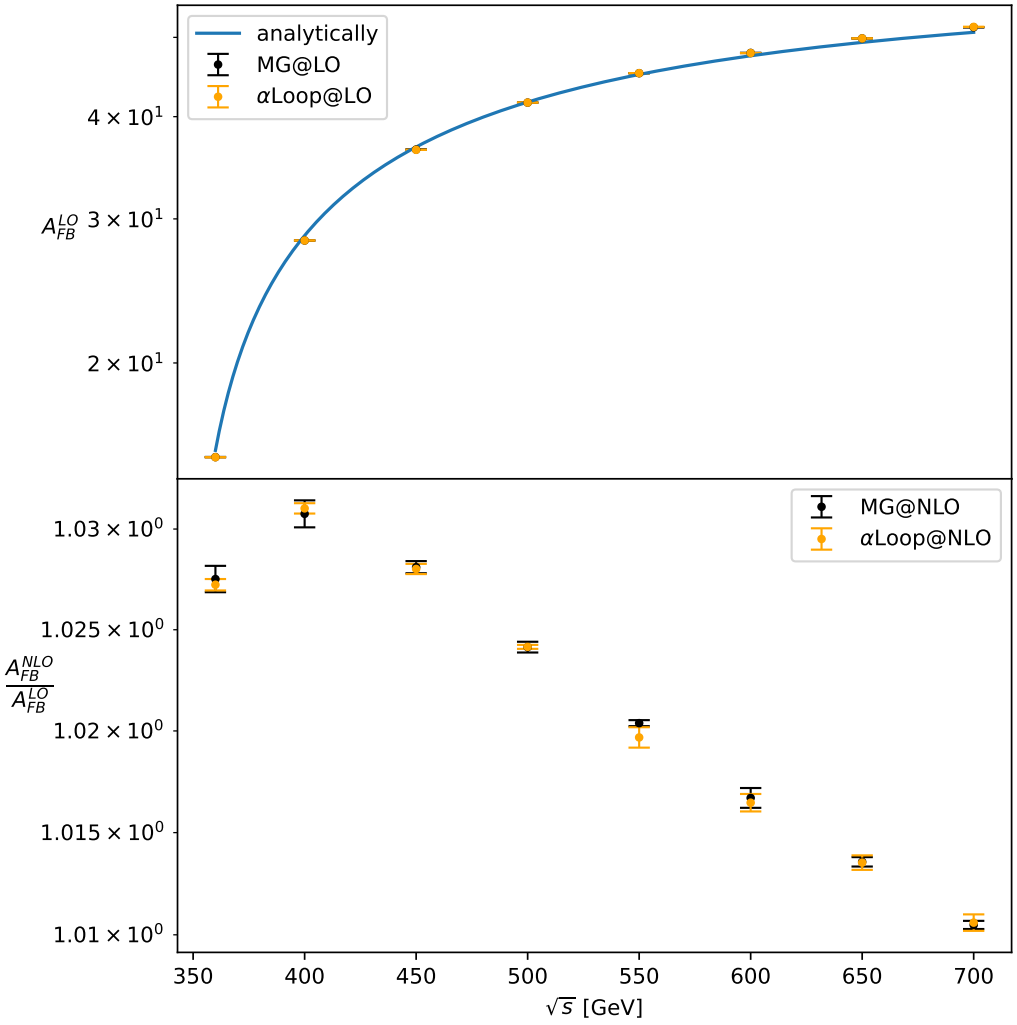

Figure 4: Forward-backward asymmetry of the process $e^+e^- \to \gamma/Z \to t\bar{t}(g)$ for various center-of-mass energies at leading (LO) and next-to-leading order (NLO) computed with the Local Unitarity implementation αLoop as well as with MadGraph5_aMC@NLO (MG) for reference. At LO the analytical result is also shown (cf. eq. (5)).

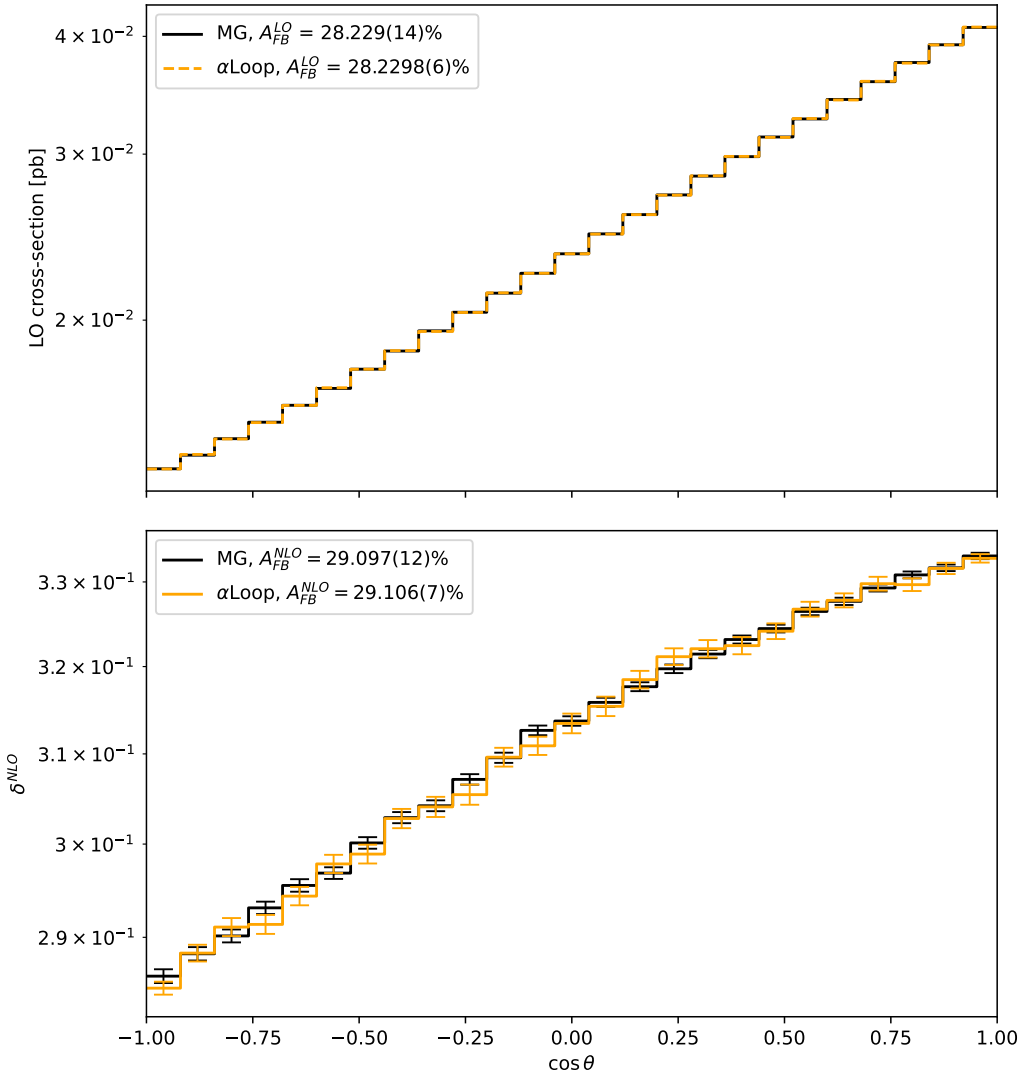

Figure 5: Angular distribution of the cross-section for the process $e^+e^- \to \gamma/Z \to t\bar{t}(g)$ approximated using 25 bins at $\sqrt{s} = 400\,\text{GeV}$. The upper graph shows the leading order contribution and the lower one the ratio δ^{NLO} of the pure NLO part and the LO part. The results have been computed with the Local Unitarity implementation αLoop as well as with MadGraph5_aMC@NLO (MG).

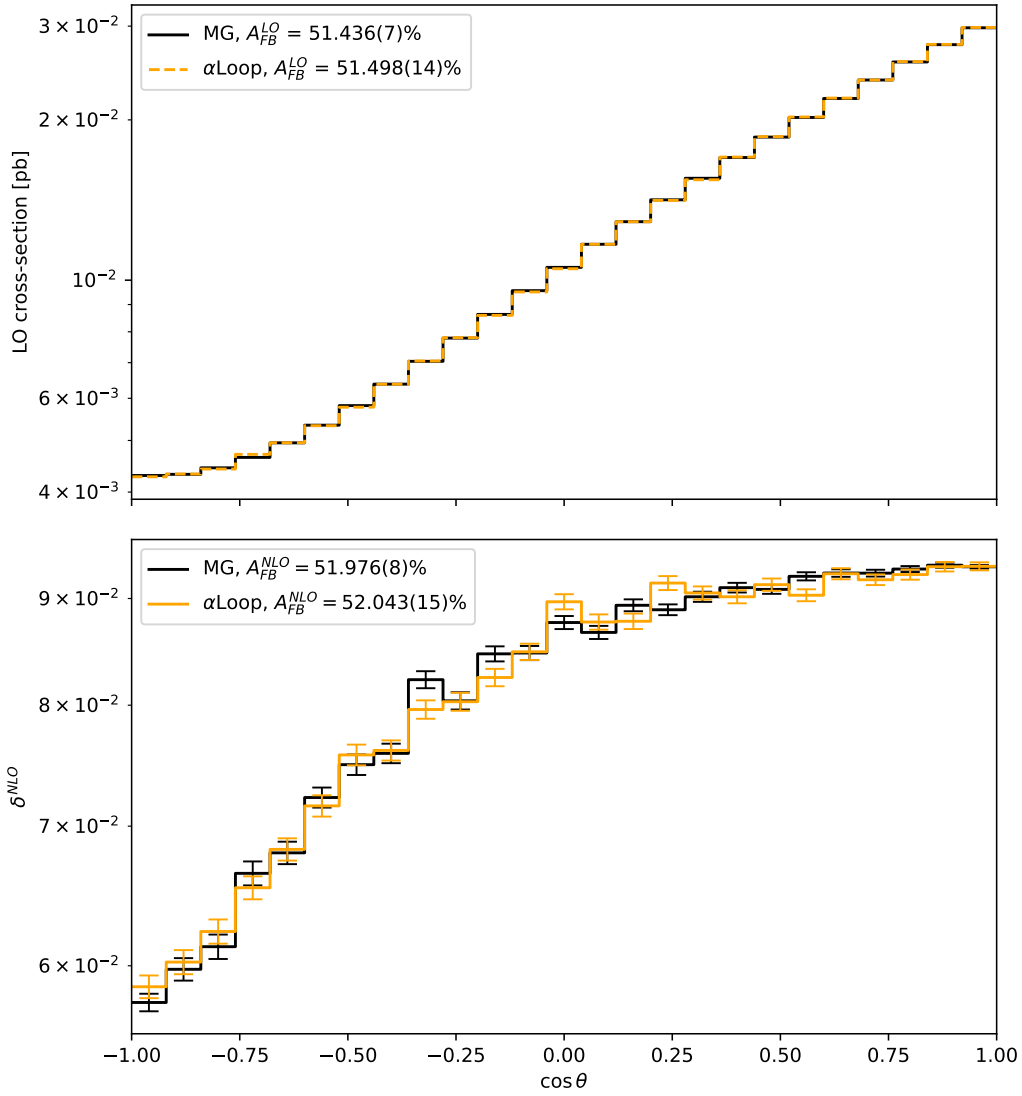

Figure 6: Angular distribution of the cross-section for the process $e^+e^- \to \gamma/Z \to t\bar{t}(g)$ approximated using 25 bins at $\sqrt{s} = 700\,\text{GeV}$. The upper graph shows the leading order contribution and the lower one the ratio δ^{NLO} of the pure NLO part and the LO part. The results have been computed with the Local Unitarity implementation αLoop as well as with MadGraph5_aMC@NLO (MG).

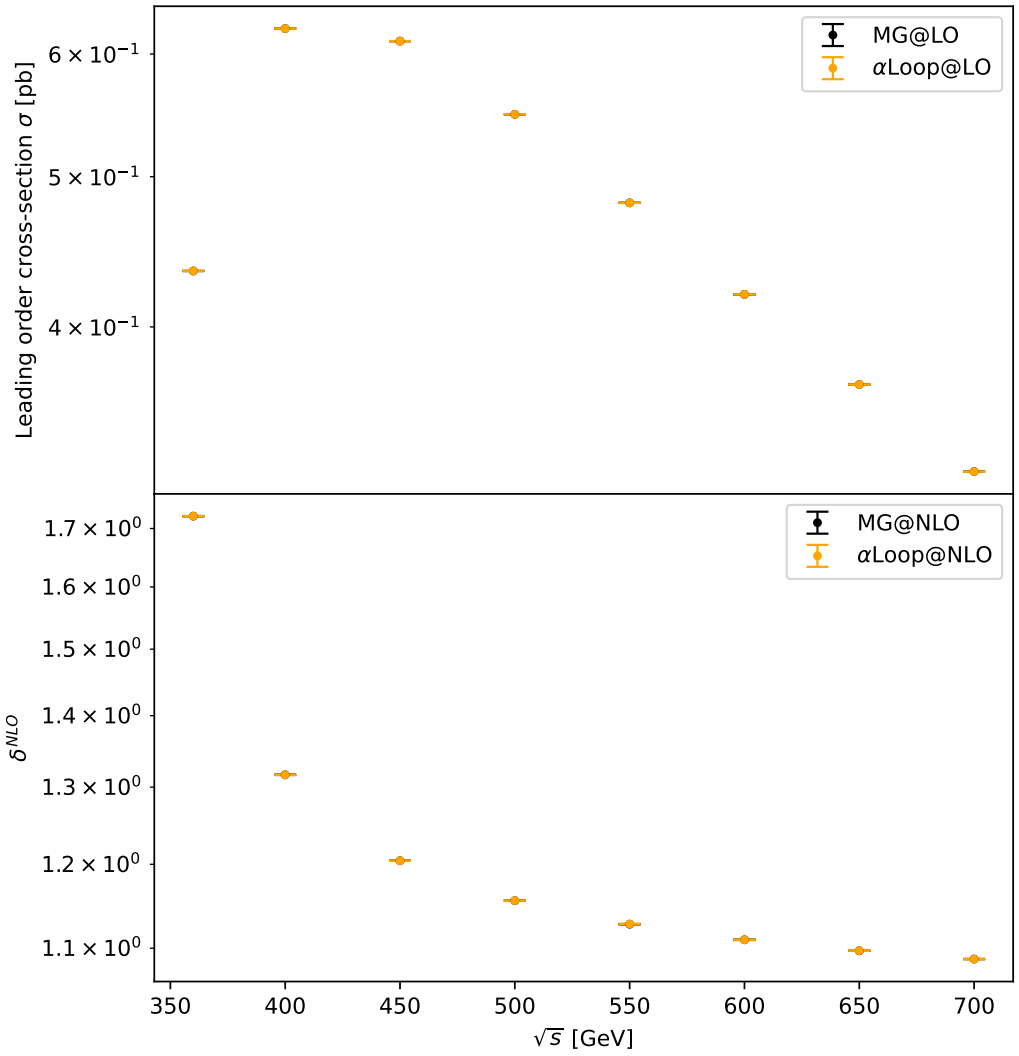

Figure 7: Differential cross-section of the process $e^+e^- \to \gamma/Z \to t\bar{t}(g)$ for various center-of-mass energies at leading and next-to-leading order computed with the Local Unitarity implementation αLoop as well as with MadGraph5_aMC@NLO (MG) for reference. The renormalization scale is fixed at the Z mass.

4 Conclusion and prospects

This work laid the ground for applying Local Unitarity (LU) to the electroweak sector by implementing the forward-backward asymmetry (AFB) and the Z boson including a scheme for handling γ^5 in dimensional regularization. The results comprise leading and next-to-leading order contributions and are in excellent agreement with MadGraph5_aMC@NLO. Of course, this is not spectacular in itself, but it already demonstrates the simple handling of observables in LU and given the high generalizability that LU offers, a treatment of higher orders is to be expected in the foreseeable future. This would be particularly desirable as it could shed light on the $2.4\,\sigma$ deviation between experiment and theory that was mentioned in the introduction.

To this end it will be important to revisit the γ^5 situation outlined in Section 2.2 as some potential issues might reveal themselves only in more complex diagrams. Another challenge that will have to be dealt with at higher order that was left untouched here is that of hadronization.

Some smaller modifications that would be helpful on the way to a full treatment of the electroweak sector are to add an option of choosing a different reference like the thrust axis for the AFB observable or to add more particles like Goldstone bosons, neutrinos or W bosons, which should be rather simple now that a γ^5 implementation is present.

References

[1] L. Chen. *Forward-backward asymmetries of the heavy quark pair production in e^+e^- collisions at $\mathcal{O}(\alpha_s^2)$*. 2021. DOI: 10.48550/ARXIV.2105.06213. URL: https://arxiv.org/abs/2105.06213.

[2] Z. Capatti, V. Hirschi, A. Pelloni, and B. Ruijl. *Local Unitarity: a representation of differential cross-sections that is locally free of infrared singularities at any order*. 2020. arXiv: 2010.01068 [hep-ph].

[3] T. Kinoshita. *Mass Singularities of Feynman Amplitudes*. 1962. DOI: 10.1063/1.1724268. eprint: https://doi.org/10.1063/1.1724268. URL: https://doi.org/10.1063/1.1724268.

[4] T. D. Lee and M. Nauenberg. *Degenerate Systems and Mass Singularities*. Mar. 1964. DOI: 10.1103/PhysRev.133.B1549. URL: https://link.aps.org/doi/10.1103/PhysRev.133.B1549.

[5] D. E. Soper. *Techniques for QCD calculations by numerical integration*. May 2000. DOI: 10.1103/physrevd.62.014009.

[6] Z. Capatti, V. Hirschi, D. Kermanschah, and B. Ruijl. *Loop-Tree Duality for Multiloop Numerical Integration*. Oct. 2019. DOI: 10.1103/physrevlett.123.151602.

[7] Z. Capatti et al. *Numerical Loop-Tree Duality: contour deformation and subtraction*. Apr. 2020. DOI: 10.1007/jhep04(2020)096.

[8] S. Catani et al. *From loops to trees by-passing Feynman's theorem*. Sept. 2008. DOI: 10.1088/1126-6708/2008/09/065.

[9] J. J. Aguilera-Verdugo et al. *Causality, unitarity thresholds, anomalous thresholds and infrared singularities from the loop-tree duality at higher orders*. 2019. DOI: 10.48550/ARXIV.1904.08389. URL: https://arxiv.org/abs/1904.08389.

[10] Z. Capatti. "Local Unitarity". In: (2021). DOI: 10.48550/ARXIV.2110.15662. URL: https://arxiv.org/abs/2110.15662.

[11] Z. Capatti, V. Hirschi, and B. Ruijl. *Local Unitarity: cutting raised propagators and localising renormalisation*. 2022. DOI: 10.48550/ARXIV.2203.11038. URL: https://arxiv.org/abs/2203.11038.

[12] G. 't Hooft and M. J. G. Veltman. *Regularization and Renormalization of Gauge Fields*. 1972. DOI: 10.1016/0550-3213(72)90279-9.

[13] J. G. Korner, D. Kreimer, and K. Schilcher. *A Practicable gamma(5) scheme in dimensional regularization*. 1992. DOI: 10.1007/BF01559471.

[14] A. Gehrmann-De Ridder. *The Standard Model of Electroweak Interactions*. June 2022.

[15] J. Alwall et al. *The automated computation of tree-level and next-to-leading order differential cross sections, and their matching to parton shower simulations*. July 2014. DOI: 10.1007/jhep07(2014)079. URL: https://doi.org/10.1007%2Fjhep07%282014%29079.

[16] R. Frederix et al. *The automation of next-to-leading order electroweak calculations*. July 2018. DOI: 10.1007/jhep07(2018)185. URL: https://doi.org/10.1007%2Fjhep07%282018%29185.

[17] E. O. Lebigot. *Uncertainties: a Python package for calculations with uncertainties*. URL: http://pythonhosted.org/uncertainties/.